Accepted Manuscript

An investigation of the thermal stability of an Mg-Dy alloy after processing by high-pressure torsion

Abdelkader Hanna, Hiba Azzeddine, Yi Huang, Djamel Bradai, Jose Maria Cabrera, Terence G. Langdon

PII: S1044-5803(19)30040-3
DOI: https://doi.org/10.1016/j.matchar.2019.03.040
Reference: MTL 9660

To appear in: *Materials Characterization*

Received date: 4 January 2019
Revised date: 13 February 2019
Accepted date: 26 March 2019

Please cite this article as: A. Hanna, H. Azzeddine, Y. Huang, et al., An investigation of the thermal stability of an Mg-Dy alloy after processing by high-pressure torsion, Materials Characterization, https://doi.org/10.1016/j.matchar.2019.03.040

An investigation of the thermal stability of an Mg-Dy alloy after processing by high-pressure torsion

Abdelkader Hanna[a], Hiba Azzeddine[b,*], Yi Huang[c,d], Djamel Bradai[e], Jose Maria Cabrera[f], Terence G. Langdon[d]

[a] Physics and Chemistry of Materials Laboratory, Department of Physics, University of Mohamed Boudiaf, M'sila, 28000, Algeria
[b] Faculty of Technology, University of Mohamed Boudiaf, M'sila, 28000, Algeria
[c] Department of Design and Engineering, Faculty of Science and Technology, Bournemouth University, Poole, Dorset BH12 5BB, UK
[d] Materials Research Group, Department of Mechanical Engineering, University of Southampton, Southampton SO17 1BJ, UK
[e] Faculty of Physics, USTHB, Algiers, Algeria.
[f] Department of Materials Science and Metallurgical Engineering, Technical University of Catalonia, Barcelona, Spain

* Corresponding author: azehibou@yahoo.fr

Abstract

An Mg-0.41Dy (wt. %) alloy was successfully processed by high-pressure tension (HPT) through 5 turns at room temperature. The evolution of the recrystallization microstructure and the texture and mechanical properties of the deformed alloy were investigated after annealing at 200 and 400 °C for 1 h using Electron Backscatter Diffraction (EBSD) and Vickers measurements. The recrystallization temperature and activation energy were evaluated using Differential Scanning Calorimetry (DSC). Processing by HPT led to significant grain refinement with an average grain size of ~0.5 ± 0.1 μm which increased to ~1.2 ± 0.8 μm after annealing at 400 °C. This slow increase in grain size at a high temperature demonstrates a good thermal stability of the microstructure. The alloy exhibited two main fiber textures after HPT processing: firstly a typical basal fiber (φ_1 = 0–360º, Φ = 0º and φ_2 = 0–60º) and secondly a fiber localized at φ_1 = 180º, Φ = 60º and φ_2 = 0–90º. These textures were retained after annealing at 400 °C. There was no change in the microhardness value after annealing at 200 °C (41 ± 1 Hv) and only a minor decrease after annealing at 400 °C (38.4 ± 0.5 Hv). The DSC results showed that the temperature associated with the recrystallization process increased with increasing heating rate and the activation energy for recrystallization was measured as ~25 kJ mol^{-1}.

Keywords: DSC; HPT; Mg-Dy alloy; microstructure; recrystallization; texture.

1. Introduction

Severe plastic deformation (SPD) techniques such as equal-channel angular pressing (ECAP) and especially high-pressure torsion (HPT) have proven effective in producing ultrafine-grained (UFG) microstructure down to the sub-micrometer level in several Mg-based alloys [1–9]. Furthermore, HPT processing generally produces smaller grains sizes than ECAP processing due to the imposition of higher strains [10]. For example, a microstructural characterization of Mg–Gd–Y–Zr alloys showed that nano-sized grains of ~72 ± 5 nm were obtained after 8 HPT turns whereas the grain size of the same alloy was ~2.2 ± 0.2 μm after 4 ECAP passes [6]. In addition, in the AZ61 alloy the average grain sizes were reported as ~0.22 μm after HPT processing at 150 °C and ~0.11 μm after HPT at room temperature [11] and there were larger grain sizes after ECAP processing at 250 °C (~1.35 μm) and 200 °C (~0.62 μm) [12].

One major advantage of HPT processing is that the grain refinement of Mg-based alloys may be achieved at room temperature without sample cracking and/or segmentation due to the high imposed hydrostatic pressure which effectively prevents propagation of fracture during torsional straining [13]. Moreover, HPT processing may significantly affect the kinetics, size and distribution of precipitates within the crystalline matrix [14, 15].

Significant improvements in the mechanical properties were reported in various Mg-based alloy caused by the grain refinement, the very high dislocation densities and the point defects that are introduced through the application of intense deformation [7, 16–18]. Furthermore, it was demonstrated that texture strengthening makes a significant contribution to the rapid increase in hardness in the early stages of deformation [8, 19]. Recent investigations have demonstrated that grain refinement plays a more significant role than dislocation strengthening since the dislocation density saturates earlier than the grain size and grain refinement continues even after the saturation of the dislocation density [16, 18]. The

continuously decreasing grain size was attributed to the annihilation of dislocations during dynamic recovery or dynamic recrystallization.

It is well established that HPT processing may produce excellent superplastic flow in numerous Mg-based alloys [11, 17, 20–24]. An exceptional elongation of 1330% at 200ºC was reported for Mg-8Li alloy after HPT processing at room temperature through 5 turns [24]. In practice, a high superplastic ductility after deformation processing requires an ultra-fine microstructure with high-angle grain boundaries and a grain size that is reasonably stable at elevated temperatures [11].

Accordingly, the ability of Mg-based alloys to maintain grain refinement during recrystallization annealing is an important requirement for achieving superplastic properties and thereby extending the use of these alloys to industrial superplastic forming applications. Improving the thermal stability of UFG materials may be achieved by reducing the grain boundary mobility and the driving force for grain growth, and this may be realized through the addition of different alloying elements or by the precipitation of second phase particles [25, 26]. The objective of the present study was to evaluate the effect of annealing temperature on the thermal stability, and specifically on the microstructure, texture and mechanical properties, of an Mg-0.41Dy alloy after processing by HPT for up to 5 turns. An earlier study reported the mechanical properties, deformation microstructures and texture of the same Mg-0.41Dy alloy after processing by HPT through 1/4 to 15 turns [8].

2. Experimental material and procedures

The as-cast Mg-0.41Dy (wt.%) alloy was provided by the Institute für Metallkunde und Metallphysik, Aachen, Germany. The alloy was produced by induction melting and casting under a protective gas atmosphere of Ar/CO_2 using preheated copper mold, followed by a heat treatment at 420 °C for 20 h.

Discs with diameters of 10 mm and thicknesses of ~0.9 mm were processed by HPT at room temperature through 5 turns. More details on the sample preparations and the processing history were given earlier [8]. After HPT processing, samples were annealed at 200 and 400 °C for 1 h in a radiation furnace under argon gas.

Electron backscatter diffraction (EBSD) measurements were performed in the rotation direction-shear direction (RD-SD) plane of the recrystallized samples using a scanning electron microscope (SEM) with a field emission gun JEOL JSM-7001F working at a voltage of 20 kV. The EBSD step size was 50 nm and the acquired raw EBSD data and orientation distribution functions (ODFs) were analyzed and calculated using MTEX software [27].

The surface morphology and chemical compositions were characterized in the RD-SD plane of the samples using an SEM coupled with energy dispersive X-ray spectroscopy (EDS). The surface preparation consisted of grinding with progressively finer SiC paper followed by mechanical polishing using a diamond solution with particle sizes ranging between 3 and 1 µm. The grain structure was revealed by subsequent etching at room temperature in an acetic-nital solution (5% HNO_3, 15% acetic acid, 20% distilled water and 60% ethanol) for 3 s.

The Vickers microhardness was measured using a SHIMADZU type HMV-2 tester. At least five indentations were made to give an average hardness value (Hv) using a load of 100 g and a dwell time of 10 s.

Differential scanning calorimetry (DSC) analyses were performed with a 2920 MDSC calorimeter under constant heating rates of 10, 20, 30 and 40 °C/min in a nitrogen atmosphere under a pressure of 1 bar. Samples of 12–19 mg were cut and placed in an aluminum holder and a separate empty aluminum holder was used as a reference.

3. Experimental results

Figure 1 illustrates the initial microstructure of the as-cast Mg-0.41Dy alloy where the grains are large and elongated with an average grain size of ~630 μm. The SEM and EDS shown in Fig. 2 reveals the presence of small amounts of second particles. The EDS results confirm the presence of two types of particles: large particle (point 1) with diameters of ~2 μm containing 16.57% of Mg and 83.43% Dy which is associated with MgDy precipitates and smaller particles that may be $Mg_{41}Dy_5$ precipitates with diameters of ~0.8 μm (point 2).

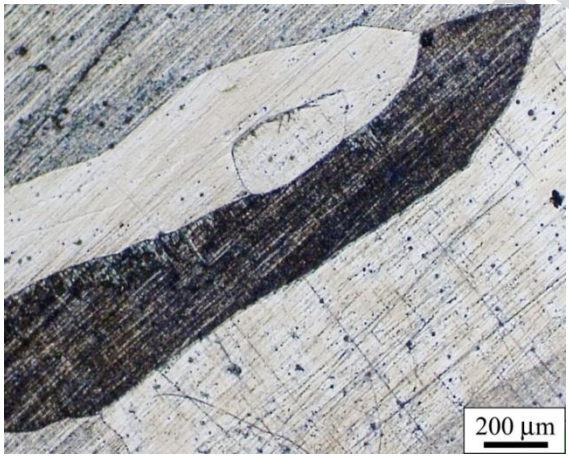

Figure 1: Optical micrograph showing the initial microstructure of the as-cast Mg-0.41Dy alloy.

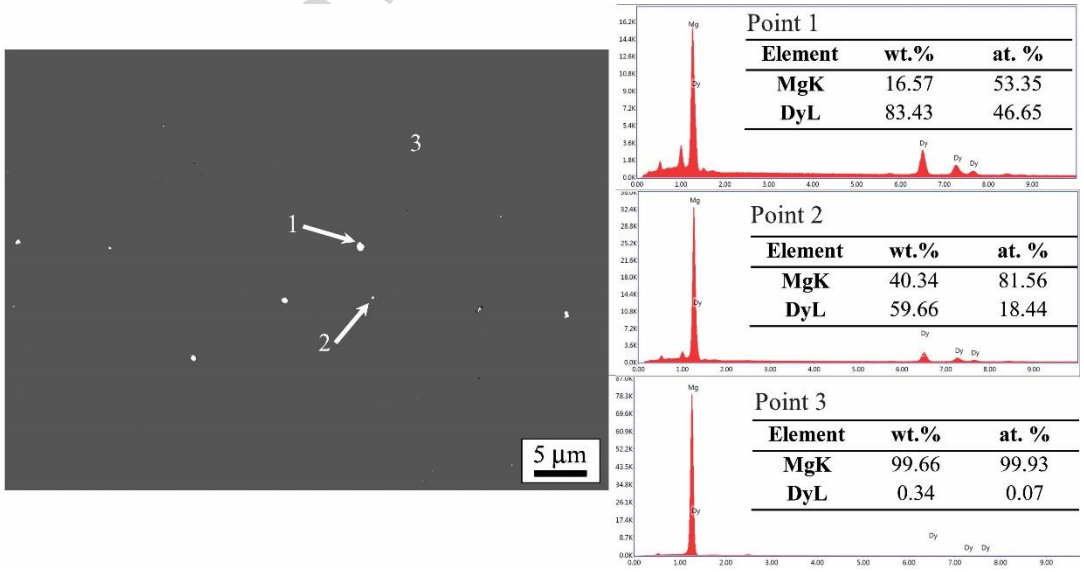

Figure 2: SEM micrograph with analysed points obtained by EDS of as-cast Mg-0.41Dy alloy.

Figure 3a presents the SEM microstructure of the Mg-0.41Dy alloy after HPT processing through 5 turns. Thus, HPT processing leads to strong grain refinement with an average grain size of ~0.5 ± 0.1 μm. A similar average grain size was reported in the same alloy measured by EBSD analysis [8]. Figure 3b indicates the presence of three types of particles with different diameters (marked by arrows and numbers) having chemical compositions summarized in Fig. 3. The concentration of Dy in these particles decreased from the as-cast state to 67.42 % (point 1), 41.86 % (point 2) and 15.36% (point 3) after HPT processing, thereby demonstrating a very significant change in composition. These results show that the HPT processing tends to decompose and dissolve the Mg-Dy particles. It is interesting to note that the smaller particles (from point 3) with sizes less than ~0.3 μm are well-dispersed in the microstructure (arrows in Fig. 3a) and have a volume fraction of ~ 0.5%.

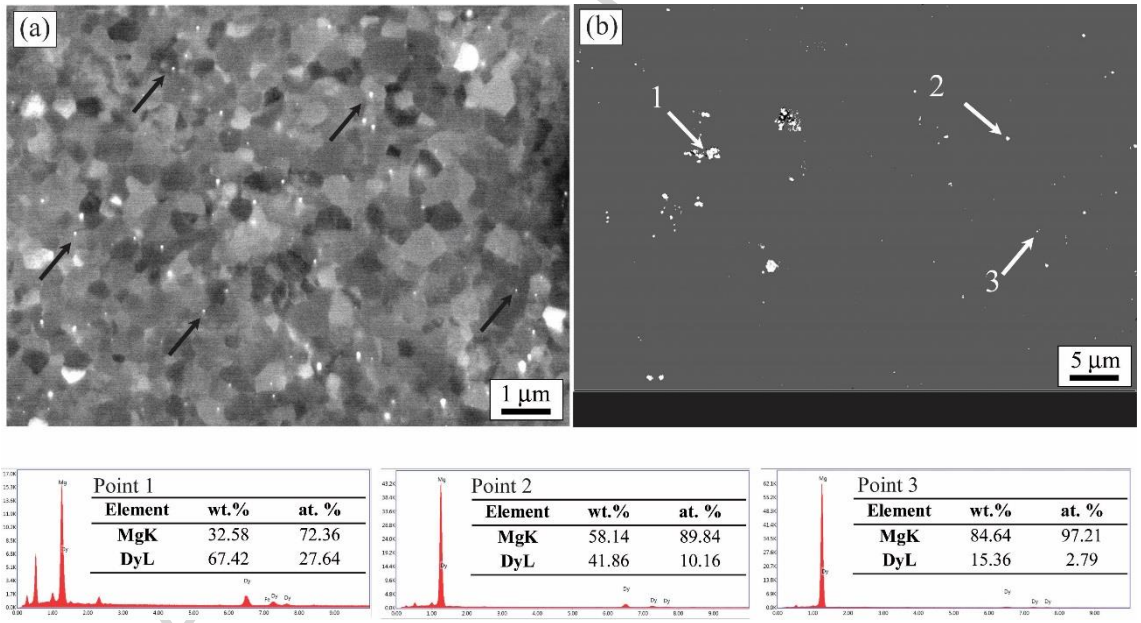

Figure 3: (a) SEM micrograph with analysed points obtained by EDS (b) of Mg-0.41Dy alloy after HPT processing through 5 turns. Arrows in Fig. 3a indicate the presence of particles of point 3.

Figure 4 illustrates the orientation imaging micrographs in inverse pole figure (IPF) maps in the RD-SD plane showing the microstructures of the Mg-0.41Dy alloy after 5 HPT

turns and annealing at 200 and 400 °C for 1 h, respectively. The distributions of grain sizes for both samples are also presented in Fig. 4. It is noted that the microstructures after annealing at 200 and 400 °C show the presence of particles with the same concentrations found in the microstructures of the deformed sample (not shown here). The variation of grains size after annealing at 200 °C shows a log-normal distribution with an average grain size of ~0.9 ± 0.2 μm. It is observed that annealing at 400 °C produces an increase in the grain size ranges leading to essentially a bimodal distribution. Nevertheless, there was only a small increase in the mean grain size to ~1.2 ± 0.8 μm.

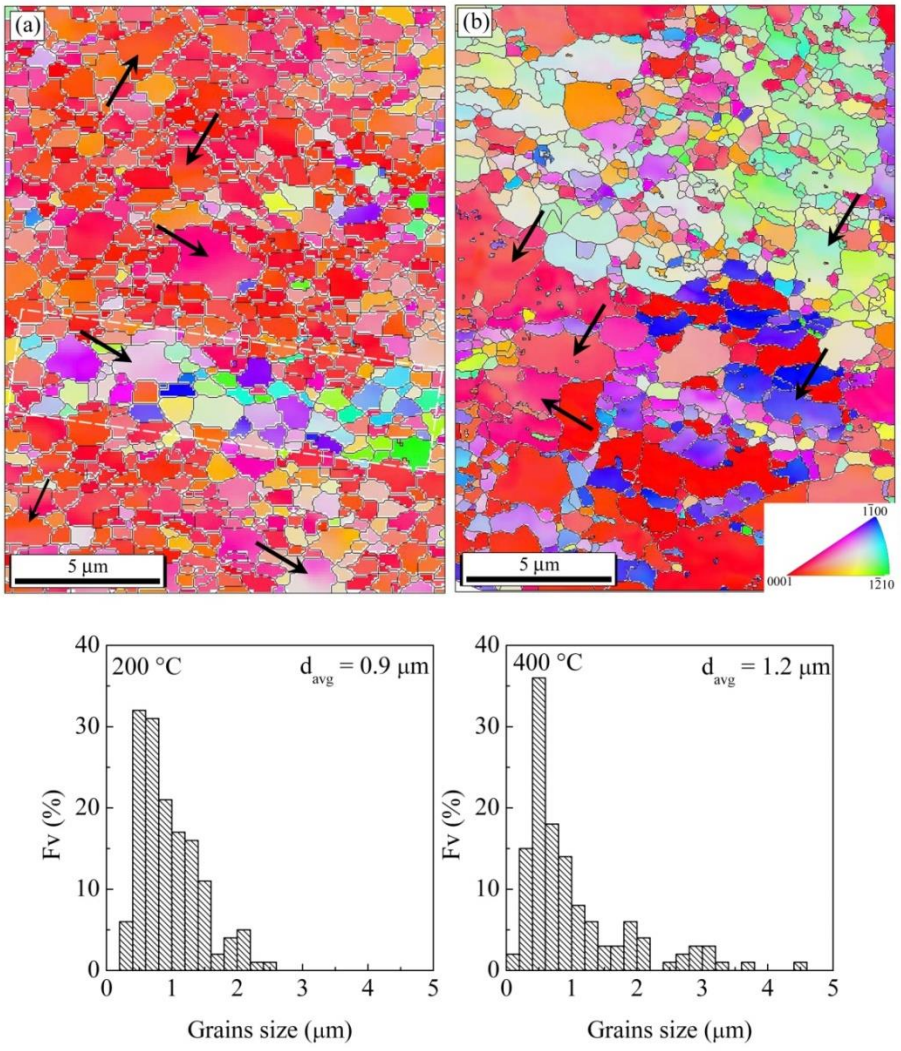

Figure 4: IPF maps and grains size distribution of the Mg-0.41Dy alloy after 5 HPT turns and annealing at 200 and 400 °C for 1 h, respectively. Arrows indicated color gradients inside some relatively large grains.

The annealed sample at 400 °C for 1 h contains different types of particles as shown in Fig. 5. Once more, the concentration of Dy in these particles seems to decrease compared with those in the as-deformed to 23.21 % (point 1), 34.49 % (point 3) showing that annealing has a great influence on the Dy element distribution. The particles with 14.88% (point 2) still exist and seem to be stable with similar size and volume fraction (~ 0.6 %) as in the deformed sample (Fig. 3, point 3).

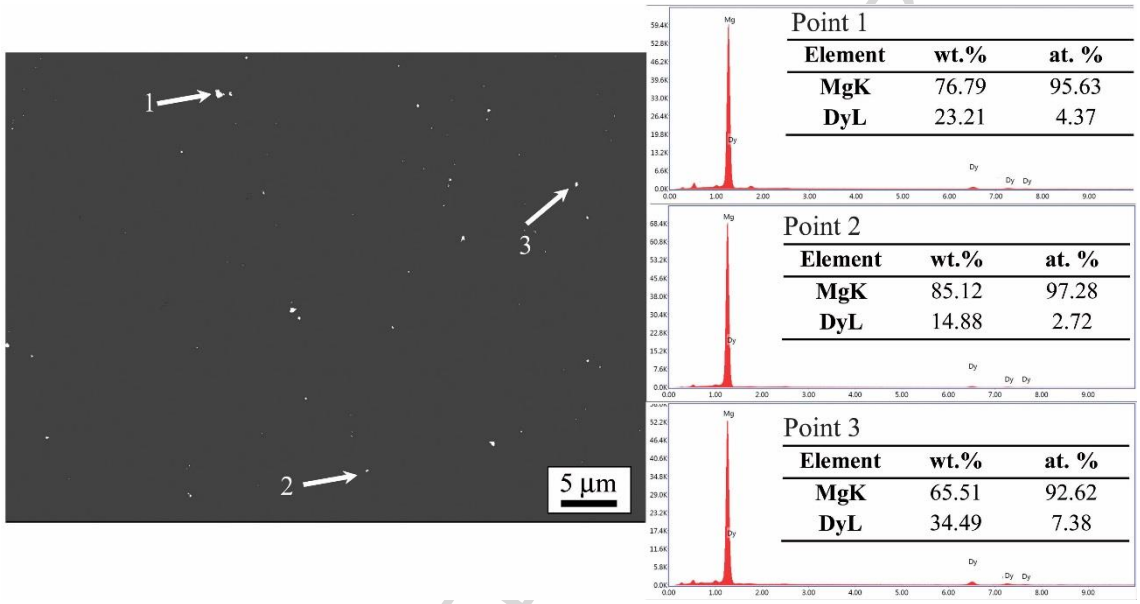

Figure 5: SEM micrograph with analysed points obtained by EDS of the Mg-0.41Dy alloy after 5 HPT turns and annealing at 400 °C for 1 h.

The distributions of the grain boundary misorientation angles are shown in Fig. 6 after 5 HPT turns and annealing for 1 h at (a) 200 and (b) 400 °C, respectively, where the solid lines show the calculated distributions for randomly oriented hexagonal materials [28]. It was reported earlier that the microstructure in the as-deformed state exhibits a high fraction of low-angle grain boundaries (LAGBs) [8] but it is readily apparent from Fig. 6 that there are predominantly high-angle grain boundaries (HAGBs) at both annealing temperatures.

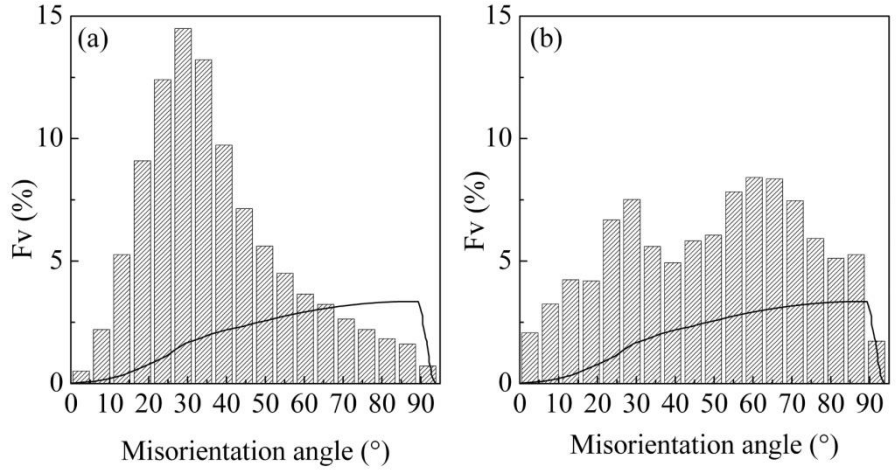

Figure 6: Misorientation angle distributions of Mg-0.41Dy alloy after 5 HPT turns and annealing for 1 h at: a) 200 and b) 400 °C.

As shown in Fig. 6, the relative fraction of LAGBs with misorientation angles below 15° was less than 9% for both annealing conditions. Inspection shows the misorientation distribution after annealing at 200 °C displays a local peak at 30° which corresponds to 30° [0001] grain boundaries (GBs) and it is known that this boundary type is responsible for the formation of a basal fiber texture [29]. Conversely, there is a shift in the number fractions of the grain boundaries towards higher angles after annealing at 400 °C.

Table 1. Evolution of the microhardness of the Mg-0.41Dy alloy processed by HPT trough 5 turns and after annealing at 200 and 400 °C for 1 h.

Sample	5 HPT	200°C 1h	400°C 1h
Hv	40.6 ± 0.9	41.0 ± 1.0	38.4 ± 0.5

The variations of the microhardness of the processed Mg-0.41Dy alloy are presented in Table 1 as a function of the annealing temperature. The microhardness for the as-cast state was ~33.5 Hv and HPT processing through 5 turns increased the microhardness to ~40.6 ±

0.9. There was no measurable change in the microhardness value after annealing at 200 °C (Hv ≈ 41.0 ± 1.0) but there was a minor decrease after annealing at 400 °C (Hv ≈ 38.4 ± 0.5).

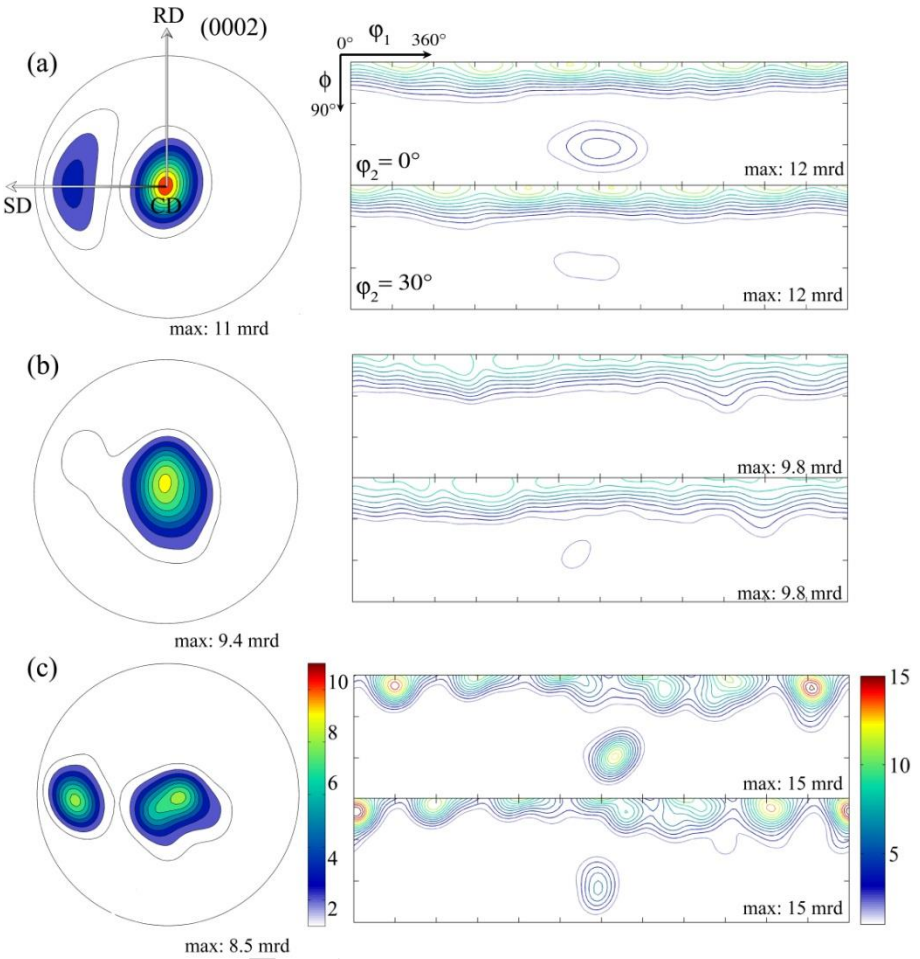

Figure 7: Recalculated pole figure (0002) and ODF sections at φ_2 = 0 and 30 ° of Mg-0.41Dy alloy after: a) 5 HPT turns and annealing for 1 h at b) 200 °C and c) 400 °C.

Figure 7 shows the texture evolution in terms of the recalculated pole figure (0002) and the ODF sections at φ_2 = 0 and 30° for the Mg-0.41Dy alloy after 5 HPT turns and annealing at 200 and 400 °C for 1 h, respectively, and Fig. 8 presents the distributions of the basal pole intensity as a function of the polar angular tilt towards SD for the same experimental conditions. Thus, this alloy exhibits two main fiber textures after 5 HPT turns, with a typical strong basal fiber (~11 mrd; multiples of random distribution) and a second weak fiber (~3 mrd) localized at φ_1 = 180º, Φ = 60º and φ_2 = 0–90º. This second fibre

corresponds to a splitting of the basal poles in the shear direction SD which is tilted by 60° towards the SD (Fig. 8). Annealing at 200 °C for 1 h leads to a typical basal texture with a disappearance of the second fiber. Nevertheless, this fiber exists after annealing at 400 °C for 1 h and has a similar intensity to the typical basal texture (~8.5 mrd) as shown in Fig. 6(c) and Fig. 8.

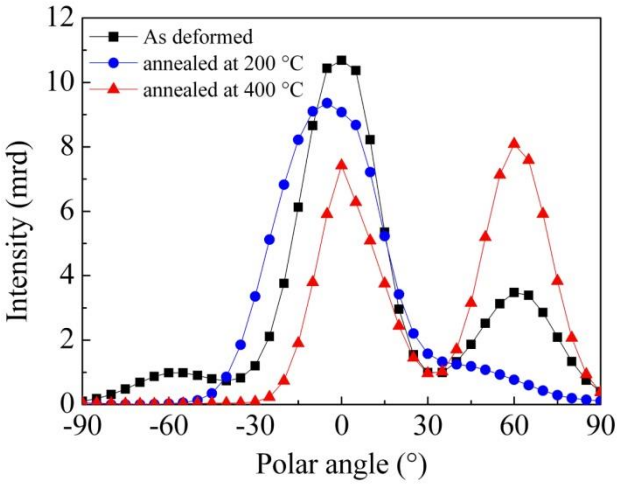

Figure 8: Basal pole intensity distribution as function of tilt towards SD of Mg-0.41Dy alloy after 5 HPT turn and annealing for 1 h at 200 and 400 °C, respectively.

Figures 9 and 10 illustrate the Schimd Factor (SF) distribution maps of the Mg-0.41Dy alloy after 5 HPT turns and annealing for 1 h at 200 and 400 °C for the basal <a>, prismatic <a>, and pyramidal <c+a> slip systems in tension along SD and RD, respectively. The grain number fractions as a function of the SF value for different slip systems are also presented in Figs 9 and 10 where the SF values are divided into low (SF <0.3) and high (SF >0.3) according to a suggested protocol [30]. Thus, grains with high FS values can accommodate larger amounts of deformation compared to those with low SF values.

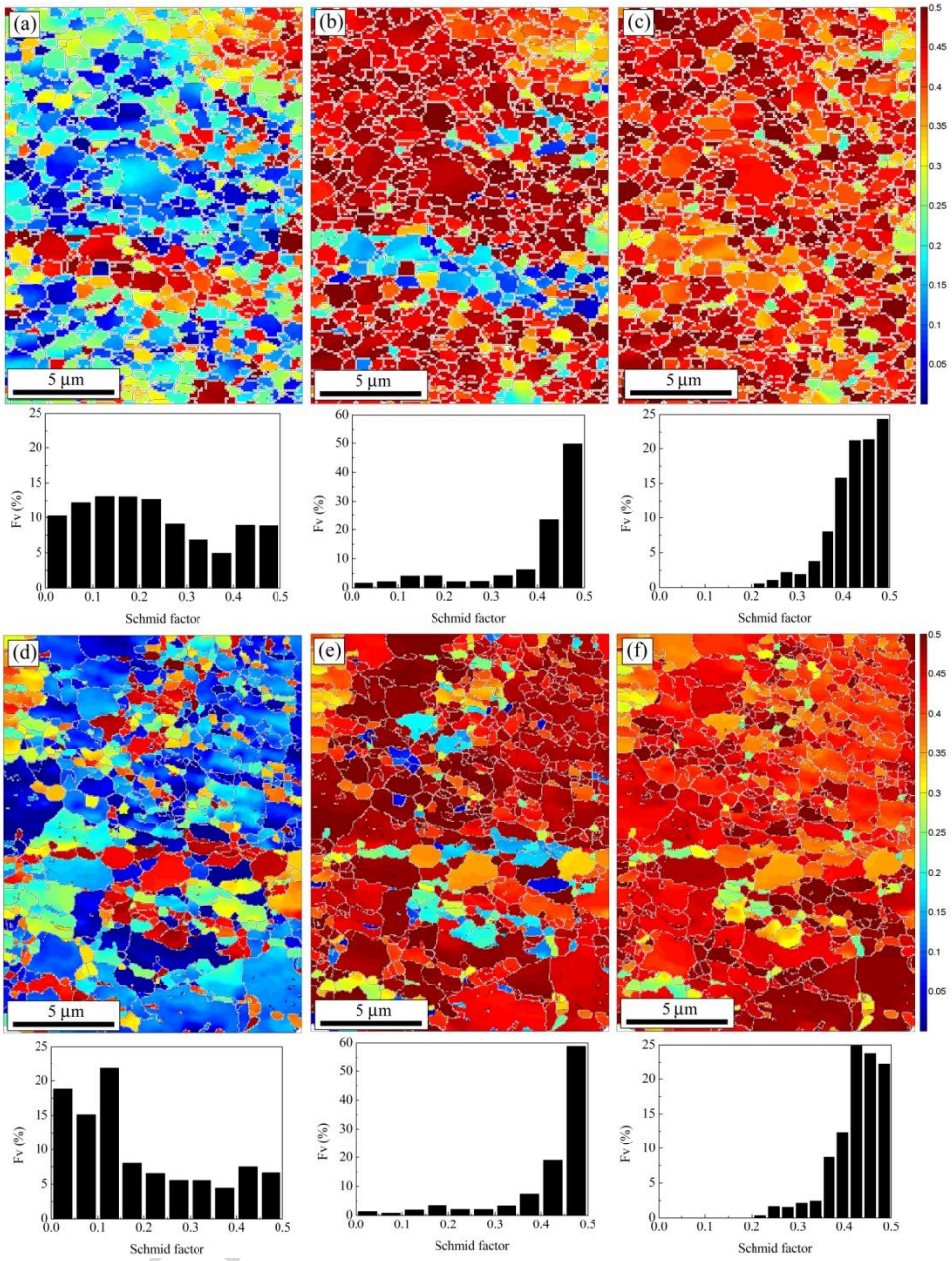

Figure 9: SF distribution maps in tension along SD for Mg-0.41Dy alloy annealed at 200 and 400 °C: (a) and (d) SF for basal <a> slip, (b) and (e) SF for prismatic <a> slip, (c) and (f) SF for pyramidal <c+a> slip.

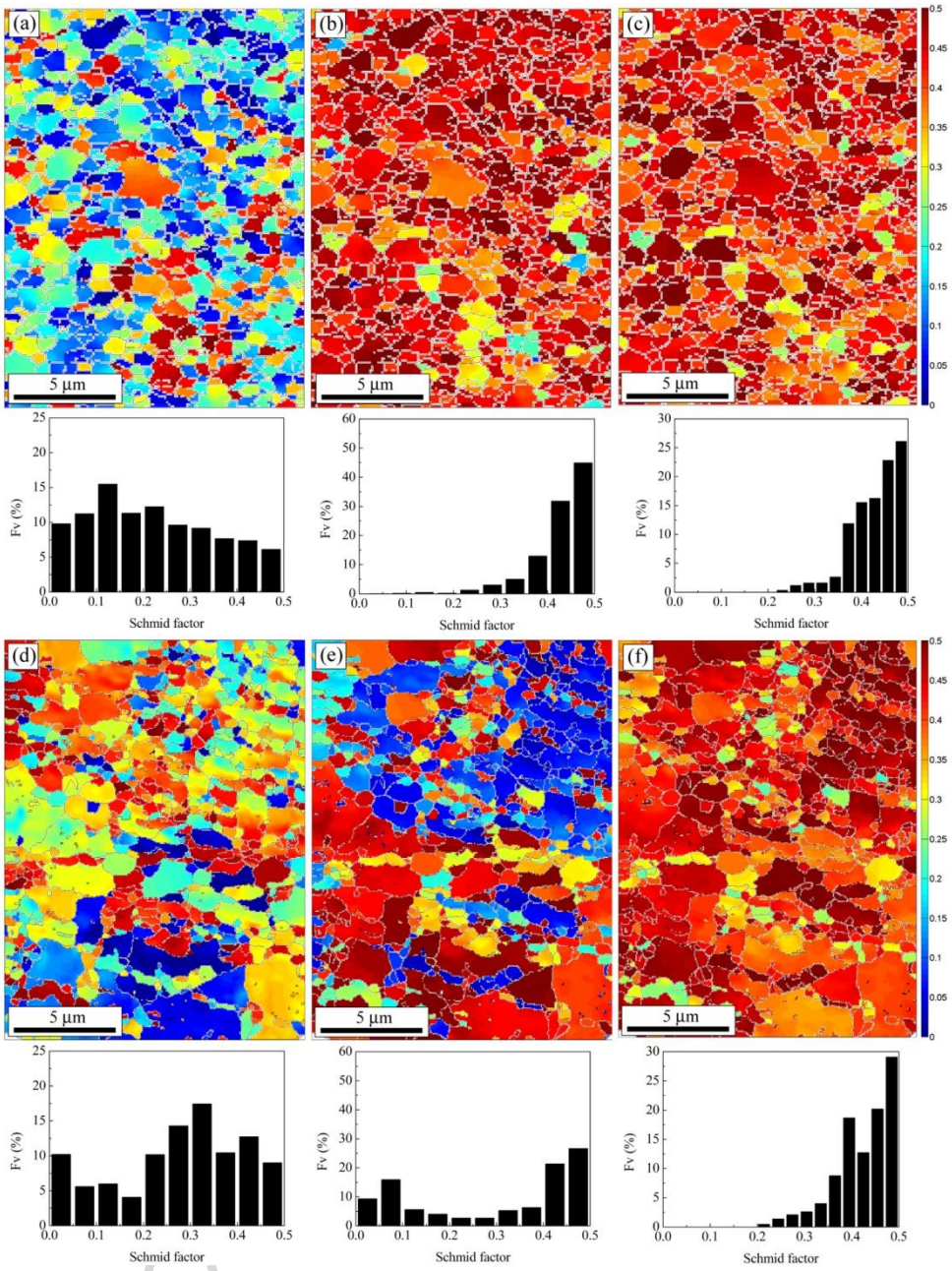

Figure 10: SF distribution maps in tension along RD for Mg-0.41Dy alloy annealed at 200 and 400 °C: (a) and (d) SF for basal <a> slip, (b) and (e) SF for prismatic < a> slip, (c) and (f) SF for pyramidal <c+a> slip.

It is apparent from Figs. 9 and 10 that the activation of different slip systems depends strongly on the grain orientations and the loading direction. Basically, grains orientated for a basal texture have low SF values for basal slip, indicating that it is less favored after annealing

at 200 and 400 °C and when the loading direction is along SD. Grains with second fiber orientation after annealing at 400 °C are not suitable for the activation of a basal slip system (Fig. 9d). Prismatic <a> and pyramidal <c+a> slip systems appear to have a high SF value for both microstructures, except for grains aligned in bands in the microstructure after annealing at 200 °C (Fig. 9b) which are not favored for <a> prismatic slip. When the loading direction is along RD, the activation of basal slip is more favoured after annealing at 400 °C (Fig. 10d) while grains with a second fiber have lower SF values for prismatic slip (Fig. 10e). It is interesting to note that the pyramidal <c+a> slip has high SF values in both microstructures and in both loading directions.

Figure 11(a) shows the DSC curves for heating rates of 10, 20, 30 and 40 °C/min for the Mg-0.41Dy alloy after 5 HPT turns. Thus, the DSC curves exhibit one single exothermic peak which corresponds to the recrystallization process and the recrystallization temperature increases with increasing heating rate within the range of ~120–200 °C. It was reported earlier that the peak temperature of recrystallization decreases with increasing numbers of HPT turns in Mg-1.44Ce (wt.%) processed by HPT at room temperature [31].

In practice, the recrystallization temperatures of cold-deformed Mg-based alloys depend strongly on the deformation strain and it was reported that at low strains ($\varepsilon < 0.1$) the recrystallization of the cold-deformed AZ31 alloy occurs only above ~200 °C whereas by increasing the strain ($\varepsilon > 0.3$) the recrystallization temperature decreases to ~150 °C [32].

Following the Boswell-Kissinger method, the activation energy for recrystallization may be obtained from the slope derived by plotting the following equation [33]:

$$ln\left(\frac{V}{T_p}\right) = C - \frac{E}{RT_p} \quad (1)$$

where V is the heating rate, E is the activation energy, T_p is the temperature associated with the peak in the DSC curve, R is the universal gas constant and C is a constant.

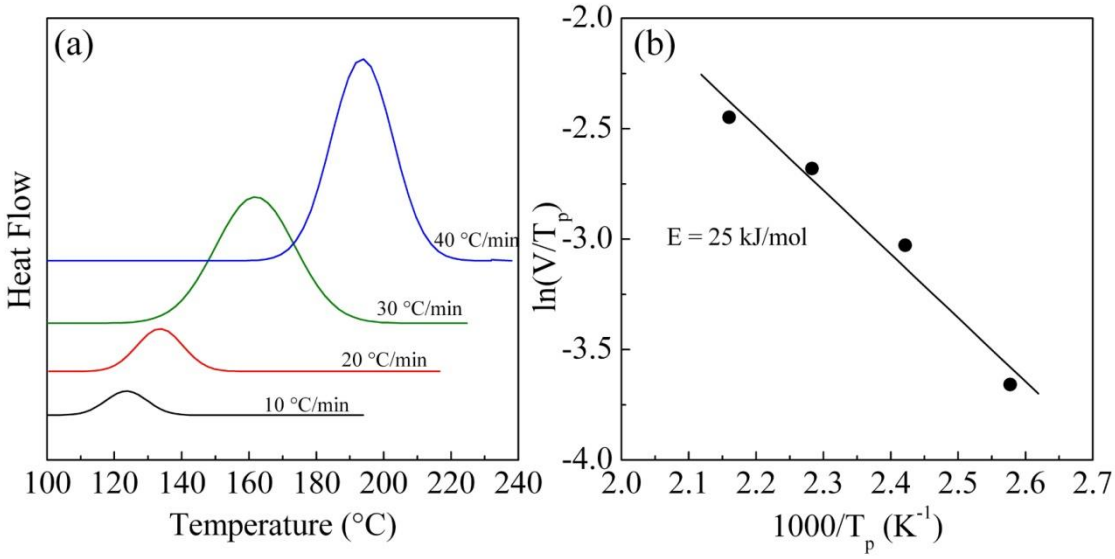

Figure 11: a) DSC curves at different heating rates and b) Boswell plots for recrystallization peak for Mg-0.41Dy alloy processed by HPT up to 5 turns.

Using eq. (1), the evolution of $\ln(V/T_p)$ as a function of $(1000/T_p\ K^{-1})$ for the recrystallization peaks are shown in Fig. 11(b) and the activation energy is estimated as ~25 kJ mol^{-1}.

4. Discussion

4.1 Significance of decomposition and recrystallization during HPT processing in the Mg-0.41Dy alloy

It is shown in this investigation that HPT processing may produce a decomposition of second particles by decreasing Dy in the $Mg_{24}Dy_5$ and MgDy particles during 5 HPT turns which lead to the formation of new particles (Fig. 3). A similar decomposition of the precipitate phases was reported in a nickel-iron-based alloy processed by HPT at room temperature and it was attributed to a mechanical mixing probably mediated by the very high hydrostatic stresses induced by HPT and localized plastic flow [34]. Additionally, the morphology and distribution of the β-$Mg_{17}Al_{12}$ phase in AZ91 and AZ80 alloys was changed

by HPT processing [23, 35]. It was also reported that ECAP processing through 2 passes leads to a disappearance of $Mg_{17}Al_{12}$ in a Mg–10Al–0.5Sb alloy [36] and a fragmentation of the $(Mg,Zn)_{12}Ce$ phase during HPT processing of an EZ33A alloy [7]. The presence of a high dislocation density in the microstructure may lead to the dissolution of second particles by enhancing the diffusivity through pipe diffusion [36]. Also, the deformed particles may become unstable due to an inherent high surface energy between the precipitates and the matrix due to the increasing strain and the change in the atomic configuration [36, 37].

Although dissolution is reported only in metastable particles, stable particles have a tendency to grow under SPD processing [37]. In fact, the $Mg_{24}Dy_5$ and MgDy precipitates existing in the present as-cast alloy with 0.41 % of Dy are unstable since the Mg-Dy phase diagram shows that the solubility of Dy in the Mg matrix is relatively high and the concentration of Dy is 24.5% and 10.2% (wt.%) at 540 and 200 °C, respectively [38]. Thus, the presence of those precipitates may be explained by their formation during the solidification process in the absence of any effective homogenization treatment.

The generation of dislocations during HPT processing leads to excellent grain refinement as shown in Fig. 3. Practically, the grain refinement mechanism in hexagonal close-packed (HCP) metals occurs through a dynamic recrystallization process [1, 8]. The OIM maps show that after annealing at 200 and 400 °C for 1 h the grain size undergoes a relatively small increase (Fig. 4). This slow increase in the mean grain size at the relatively high temperature of 400 °C demonstrates that the microstructure has a good thermal stability. Moreover, the microhardness values in the deformed and annealed state are very similar as shown in Table 1.

The activation energy of recrystallization in the present study was found to be ~25 kJ mol^{-1} (Fig.11b). This value is lower than the value for self-diffusion through the lattice in Mg (~135 kJ mol^{-1}) or for boundary self-diffusion (~92 kJ mol^{-1}) [39]. Very recently, a similar

value of the activation energy (~22.2 kJ mol^{-1}) was reported for pure Mg processed by ECAP [40]. However, the activation energy of recrystallization was reported earlier as lying in the range of ~72–87 kJ mol^{-1} in an Mg-Ce alloy processed by HPT at room temperature [31].

The low activation energy found in the present study could be attributed to the ability of SPD processing to introduce high deformation leading to more nucleation sites including HAGBs, a high concentrations of vacancies and/or vacancy agglomerates [41]. On the other hand, it was suggested that ultrafine grain sizes and strong basal texture may cause a decrease in the activation energy of recrystallization [42] which is the case in the present alloy. Although the as-deformed sample has already dynamically recrystallized, it is expected that during heating the pre-existing recrystallized grains will grew immediately and new statically recrystallized grains are nucleated and grow at the same time so that a lower activation energy is needed for the transformation.

Unfortunately, there are few results available in the literature dealing with the activation energy of recrystallization in severely-deformed Mg-based alloys and therefore there is no complete understanding of the recrystallization mechanisms.

The good thermal stability in this alloy is attributed to the presence of particles, most probably to those containing 15.36% of Dy, since they are stable, very small and well-dispersed in the microstructures of the deformed and annealed samples (Figs. 3 and 5) and therefore they restrict grain growth by pinning the grain boundaries. It is well known that stable dispersed particles exert a retarding force by solute drag and/or Zener pinning on grain boundary mobility and grain growth [43–45]. A much larger grain size of ~5 μm was reported in an AZ31 alloy after HPT processing and annealing at 400 °C for 30 min [46]. The variation of grain size as a function of annealing temperature for the AZ61 alloy processed by HPT through 5 turns at 150 °C and then annealed for 1 h at temperatures from 25 to 250 °C

revealed excellent grain stability up to 200 °C (~0.3 μm) but there was significant grain growth to ~1.2 μm at 250 °C [11].

Nevertheless, both OIM maps show color gradients within some relatively large grains, as denoted by the arrows in Fig. 4, and this indicates that recrystallization is not complete after annealing at 200 or even 400 °C for 1 h. By contrast, the DSC results show that the recrystallization process may occur at lower temperatures of 120–200 °C and these grains are fragments that have not fully refined; similar observation were also reported in other studies [26, 47]. This phenomenon was attributed to the disappearance of the sub-structure due to dislocation recovery or recombination under high temperature conditions leading to the occurrence of exceptionally large grains [26].

Another microstructural feature for the sample annealed at 200 °C is that grains with different orientations are aligned in bands. The nucleation and growth of these randomly oriented grains is indicative of shear banding and recrystallization at shear band is known as a mechanism responsible for random texture in Mg-Rare Elements (RE) alloys [48–50]. Unfortunately, it was not possible to directly confirm the presence of shear bands after processing for 5 turns but it is known that at high strains the recrystallized grains in Mg-based alloy are formed along HAGBs and within shear bands [32].

4.2 Development of a deformation texture in the Mg-0.41Dy alloy

The evolution of the deformation texture in the present work is different from earlier reports for pure Mg [51] or Mg-RE alloys [52] processed by HPT at room temperature. Usually after HPT processing there is a typical basal fiber texture where the basal (0002) planes are parallel to the shear (SD, RD) plane [51] while the textures of Mg-RE (RE=Nd, Ce) alloys after HPT processing are characterized by an asymmetric basal texture shifted by 15° towards the shear direction [52]. The texture of the as-cast Mg-0.41Dy alloy was

considered random and the deformation texture developed starting from 1 HPT turn but appeared to saturate after 5 HPT turns because of dynamic recrystallization [8]. Generally, the dynamic recrystallization in Mg-based alloys leads to the same deformation texture [44, 53–55].

It has been shown that the development of a basal texture during the early stages of HPT processing is due to the activation of extension twinning $\{10\bar{1}2\}\langle 10\bar{1}\bar{1}\rangle$ where the c-axis of the crystals is re-oriented by 86.8° so that it is nearly parallel to the loading direction [8, 56]. The development of a weak second fiber in the present alloy, in which the basal poles are tilted about 60° towards the SD (Fig. 7), may be attributed to the activation of <a> prismatic slip and <c+a> pyramidal slip [8] during HPT processing at room temperature. The activation of <a> prismatic slip and <c+a> pyramidal slip is usually hard in conventional Mg-based alloy deformed at room temperature [57] but it becomes easier in Mg-RE alloys because of the effect of the RE elements in decreasing the stacking fault energy and providing an ability for cross-slip as the solutes diffuse in the dislocation cores [8, 58].

In practice, the origin of the strong texture during dynamic recrystallization is not well understood. For many years the strong basal texture observed in Mg-based alloys upon dynamic recrystallization was attributed to the activation of basal slip and dynamic recovery mechanisms [59]. Thus, basal slip allows the basal plane to mitigate stress by reorienting the c-axis normal to the loading direction, while dynamic recovery allows dislocations to rearrange into subgrains while maintaining the basal plane parallel to the main loading axis [55, 59, 60]. By contrast, recent studies revealed that the grain boundary properties are a fundamental characteristic in the dynamic recrystallization of Mg-based alloy [59, 61] and it was proposed that the strong segregation of RE elements to the grains boundaries may homogenize the grain boundary energy and affect the boundary mobility, thereby reducing the preferred selection of special 30° [0001] boundaries and allowing other orientations to

develop and stabilize to produce a more randomized texture [61]. However, as reported earlier [8] and consistent with the present study, the grains with 30° [0001] boundaries remain dominant (Fig. 5) with an enhancement of the basal fiber orientation in the deformed state and in the annealed state after annealing at 200 °C. In this case the development of a basal texture in the Mg-0.41Dy alloy is attributed to an insufficient Dy segregation at the grain boundaries for the nucleation of dynamic recrystallization.

It is well known that the final recrystallization texture depends either on the oriented nucleation of new grains or the subsequent favorable growth of grains with specific orientations or on both of these effects [62]. It was demonstrated by quasi-in-situ EBSD measurements that cold rolled Mg-0.4Zn and Mg-0.1Ca alloys (wt.%) annealed at 350 °C for 900 s develop a weak recrystallization texture in the early stage of recrystallization but this is gradually replaced by a strong basal texture via the preferential growth of recrystallized grains with specific orientations [63]. Nevertheless, as shown in Fig. 6, the recrystallization textures are slightly weaker than the deformed textures but they are retained and no new components are observed. Generally, the recrystallization annealing treatment after deformation does not significantly alter the deformation texture of Mg-based alloys [44, 53, 54] and this is explained by the quasi-complete dynamic recrystallization occurring in HPT processing.

4.3 The deformation modes in the Mg-0.41Dy alloy

The present work demonstrates that the grains sizes of the Mg-0.41Dy alloy are reasonably stable and the microstructures have HAGBs which suggest this alloy is a good candidate material for exhibiting high ductilities and possibly even superplastic behavior.

The relative activation of each deformation mode in Mg-based alloys is fundamental for predicting the deformation behavior. The Schmid factor (SF) is frequently applied to analyze the possibility of the activation of deformation modes with different values of the

critical resolved shear stress (CRSS) with respect to the loading direction [64]. For example, it was reported that the macroscopic yield stress is largely affected by the CRSS of the deformation mode having the highest value of the SF [65].

The evolution of SF values shown in Figs. 8 and 9 supports that at elevated temperatures pyramidal <c+a> slip becomes more dominant as it supplies strain accommodation along the c-axis of grains [57, 66]. It was reported that the activation of non-basal slip is beneficial for enhancing the ductility of Mg alloys [67]. Therefore, it may be speculated that the Mg-0.41Dy alloy will have high ductility under tensile loads (RD and SD) due to the activation of different deformation modes.

5. Summary and conclusions

1. Experiments were conducted on an Mg-0.41Dy (wt. %) alloy to evaluate the thermal stability after processing by HPT through 5 turns at room temperature. Following HPT processing, samples were annealed for 1 h at temperatures of 200 and 400 ºC.

2. Processing by HPT produces a significant refinement in grain size from an initial value larger than ~2 mm to a value of ~0.5 ± 0.1 μm. Following annealing, the grain sizes increased slightly to ~0.9 ± 0.2 and ~1.2 ± 0.8 μm at annealing temperatures of 200 and 400 ºC, respectively. These results demonstrate a good thermal stability.

3. After HPT processing, there was a typical basal fiber (φ_1 = 0–360º, Φ = 0º and φ_2 = 0–60º) associated with a second fiber localized at φ_1 = 180º, Φ = 60º and φ_2 = 0–90º. These textures were retained after subsequent annealing at 400 °C for 1 h.

4. The microhardness values were stable after annealing at 200 °C but there was a slight decrease in hardness after annealing at 400 °C. The recrystallization temperature was measured in the range of ~120–200 °C and it increased with increasing heating rate. The activation energy for recrystallization was ~25 kJ mol^{-1}.

5. HPT processing and an annealing treatment leads to significant decomposition of second particles by the decreasing Dy element in the different types of particles that are present in this alloy.

6. The good stability of the Mg-0.41Dy alloy after annealing up to 400 °C is attributed to the occurrence of dynamic recrystallization during HPT processing, the presence of particles and the effect of the Dy elements on grain boundary mobility.

Acknowledgements

HA gratefully acknowledges the help of Dr. Talal Al-Samman, Institute für Metallkunde und Metallphysik (IMM-RWTH), Aachen, Germany, in supplying the Mg-RE alloys. AH wishes to heartily thank the staff of the Biomaterials Research Group in Polytecnia ETSEIB, Universidad Politécnica de Cataluña (UPC), for their support in the DSC analysis. Two of the authors (YH and TGL) were supported by the European Research Council under ERC Grant Agreement No. 267464-SPDMETALS.

References

[1] R.B. Figueiredo, T.G. Langdon, Grain refinement and mechanical behavior of a magnesium alloy processed by ECAP, J. Mater. Sci. 45 (2010) 4827–4836. https://doi.org/10.1007/s10853-010-4589-y

[2] P. Minárik, J. Veselý, R. Král, J. Bohlen, J. Kubásek, M. Janeček, J. Stráská. Exceptional mechanical properties of ultra-fine grain Mg-4Y-3RE alloy processed by ECAP. Mater. Sci. Eng., A 708 (2017) 193–198. https://doi.org/10.1016/j.msea.2017.09.106

[3] J. Čížek, P. Hruška, T. Vlasák, M. Vlček, M. Janeček, P. Minárik, T. Krajňák, M. Šlapáková, M. Dopita, R. Kužel, T. Kmječ, J.G. Kim, H.-S. Kim, Microstructure development of ultra fine grained Mg-22 wt%Gd alloy prepared by high pressure torsion, Mater. Sci. Eng. A 704 (2017) 181–191. https://doi.org/10.1016/j.msea.2017.07.100

[4] W.T. Sun, C. Xu, X.G. Qiao, M.Y. Zheng, S. Kamado, N. Gao, M.J. Starink, Evolution of microstructure and mechanical properties of an as-cast Mg- 8.2Gd-3.8Y-1.0Zn-0.4Zr alloy processed by high pressure torsion, Mater. Sci. Eng. A 700 (2017) 312–320. https://doi.org/10.1016/j.msea.2017.05.115

[5] W.T. Sun, X.G. Qiao, M.Y. Zheng, C. Xu, N. Gao, M.J. Starink, Microstructure and mechanical properties of a nanostructured Mg-8.2Gd-3.8Y-1.0Zn-0.4Zr supersaturated solid solution prepared by high pressure torsion, Mater. Des. 135 (2017) 366–376. https://doi.org/10.1016/j.matdes.2017.09.048

[6] R. Alizadeh, R. Mahmudi, P.H.R. Pereira, Y.Huang, T.G. Langdon. Microstructural evolution and superplasticity in an Mg–Gd–Y–Zr alloy after processing by different SPD techniques. Mater. Sci. Eng. A 682 (2017) 577–585. https://doi.org/10.1016/j.msea.2016.11.080

[7] K. Bryla, J. Morgiel, M. Faryna, K. Edalati, Z. Horita. Effect of high-pressure torsion on grain refinement, strength enhancement and uniform ductility of EZ magnesium alloy. Mater. Lett. 212 (2018) 323–326. https://doi.org/10.1016/j.matlet.2017.10.113

[8] A. Hanna, H. Azzeddine, R. Lachhab, T. Baudin, A.L. Helbert, F. Brisset, Y. Huang, D. Bradai, T. G. Langdon. Evaluating the textural and mechanical properties of an Mg-Dy alloy processed by high-pressure torsion. J. Alloys Compd. 778 (2019) 61–71. https://doi.org/10.1016/j.jallcom.2018.11.109

[9] R.B. Figueiredo, T.G. Langdon, Processing of magnesium and its alloys by high-pressure torsion: An overview. Adv. Eng. Mater. (2019) 1801039 (in press). https://doi.org/10.1002/adem.201801039

[10] A.P. Zhilyaev, T.G. Langdon, Using high-pressure torsion for metal processing: fundamentals and application, Prog. Mater. Sci. 53 (2008) 893–979. https://doi.org/10.1016/j.pmatsci.2008.03.002

[11] Y. Harai, M. Kai, K. Kaneko, Z. Horita, T.G. Langdon, Microstructural and mechanical characteristics of AZ61magnesium alloy processed by high-pressure torsion, Mater. Trans. 49 (2008) 76–83. https://doi.org/10.2320/matertrans.ME200718

[12] Y. Miyahara, Z. Horita and T. G. Langdon. Exceptional superplasticity in an AZ61 magnesium alloy processed by extrusion and ECAP. Mater. Sci. Eng. A 420 (2006) 240–244. https://doi.org/10.1016/j.msea.2006.01.043

[13] Y. Huang, R.B. Figueiredo, T. Baudin, F. Brisset, T.G. Langdon, Evolution of strength and homogeneity in a magnesium AZ31 alloy processed by high-pressure torsion at different temperatures, Adv. Eng. Mater. 14 (2012) 1018-1026. https://doi.org/10.1002/adem.201200016

[14] J. Čížek, I. Procházka, B. Smola, I. Stulíková, R. Kužel, Z. Matěj, V. Cherkaska, R.K. Islamgaliev, O. Kulyasova. Microstructure and Thermal Stability of Ultra Fine Grained Mg-

based Alloys Prepared by High Pressure Torsion. Mater. Sc. Forum 503-504 (2006) 149-154. https://doi.org/10.1016/j.msea.2006.01.177

[15] Y. I. Bourezg, H. Azzeddine, L. Hennet, D. Thiaudière, Y. Huang, D. Bradai, T. G. Langdon. The sequence and kinetics of pre-precipitation in Mg-Nd alloys after HPT processing: A synchrotron and DSC study. J. Alloys Compd. 719 (2017) 236–241. https://doi.org/10.1016/j.jallcom.2017.05.166

[16] J. Stráská, M. Janeček, J. Gubicza, T. Krajňák, E. Y. Yoon, H. S. Kim. Evolution of microstructure and hardness in AZ31 alloy processed by high pressure torsionMater. Sci. Eng. A 625 (2015) 98–106. https://doi.org/10.1016/j.msea.2014.12.005

[17] R. Alizadeh, R. Mahmudi, A.H.W. Ngan, Y. Huang, T.G. Langdon, Superplasticity of a nano-grained Mg-Gd-Y-Zr alloy processed by high-pressure torsion, Mater. Sci. Eng. A 651 (2016) 786–794. https://doi.org/10.1016/j.msea.2015.10.094

[18] J. Gu, X. Yang, S. Ni, M. Song, Structural and hardness evolution of pure magnesium subjected to high pressure torsion, Rare Metal Mat. Eng. 47 (2018) 1347–1351. https://doi.org/10.1016/S1875-5372(18)30133-4

[19] X.G. Qiao, Y.W. Zhao, W.M. Gan, Y.C. Ming, Y. Zheng, K. Wu, N. Gao, M.J. Starink, Hardening mechanism of commercially pure Mg processed by high pressure torsion at room temperature, Mater. Sci. Eng. A 619 (2014) 95–106. https://doi.org/10.1016/j.msea.2014.09.068

[20] O.B. Kulyasova, R.K. Islamgaliev, A.R. Kil'mametov, R.Z. Valiev, Superplastic behavior of magnesium-based Mg–10 wt % Gd Alloy after severe plastic deformation by torsion, Phys. Metals Metallog. 101 (2006) 585–590. https://doi.org/10.1134/S0031918X0606010X

[21] S.A. Torbati-Sarraf, T.G. Langdon, Properties of a ZK60 magnesium alloy processed by high-pressure torsion, J. Alloy. Compd. 613 (2014) 357–363. https://doi.org/10.1016/j.jallcom.2014.06.056

[22] M. Kai, Z. Horita, T.G. Langdon, Developing grain refinement and super-plasticity in a magnesium alloy processed by high pressure torsion, Mater. Sci. Eng. A 488 (2008) 117–124. https://doi.org/10.1016/j.msea.2007.12.046

[23] A.S.J. Al-Zubaydi, A.P. Zhilyaev, S.C. Wang, P.A.S. Reed, Superplastic behavior of AZ91magnesium alloy processed by high-pressure torsion, Mater. Sci. Eng. A 637 (2015) 1–11. https://doi.org/10.1016/j.msea.2015.04.004

[24] H. Matsunoshita, K. Edalati, M. Furui, Z. Horita, Ultrafine-grained magnesium–lithium alloy processed by high-pressure torsion: low-temperature superplasticity and potential for hydroforming, Mater. Sci. Eng. A 640 (2015) 443–448. https://doi.org/10.1016/j.msea.2015.05.103

[25] J. Cizek, I. Prochazka, B. Smola, I. Stulíkova, R. Kuzel, Z. Matej, V. Cherkaska, R.K. Islamgaliev, O. Kulyasova, Microstructure and thermal stability of ultrafine grained Mg-based alloys prepared by high-pressure torsion, Mater. Sci. Eng. A 462 (2007) 121–126. https://doi.org/10.1016/j.msea.2006.01.177

[26] L. Tang, Y. Zhao, R.K. Islamgaliev, R.Z. Valiev, Y.T. Zhu. Microstructure and thermal stability of nanocrystalline Mg-Gd-Y-Zr alloy processed by high pressure torsion. J. Alloys Compd. 721 (2017) 577–585. https://doi.org/10.1016/j.jallcom.2017.05.164

[27] R. Hielscher, H. Schaeben, A novel pole figure inversion method: specification of the MTEX algorithm, J. Appl. Cryst. 41 (2008) 1024–1037. https://doi.org/10.1107/S0021889808030112

[28] A. Morawiec. Misorientation-Angle Distribution of Randomly Oriented Symmetric Objects. J. Appl. Crystallogr. 28 (1995) 289–293. https://doi.org/10.1107/S0021889894011088

[29] J.A. del Valle, M.T. Perez-Prado, O.A. Ruano, The distribution of disorientation angles in a rolled AZ31 Mg alloy, Rev. Metal. Madr. 38 (2002) 353–357. DOI: 10.3989/revmetalm.2002.v38.i5.419

[30] J.J. Jonas, S. Mu, T. Al-Samman, G. Gottstein, L. Jiang, E. Martin, The role of strain accommodation during the variant selection of primary twins in magnesium, Acta Mater. 59 (2011) 2046–2056. https://doi.org/10.1016/j.actamat.2010.12.005

[31] Y.I. Bourezg, H. Azzeddine, Y. Huang, D. Bradai, T.G. Langdon (2017) Investigation of recrystallization kinetics by DSC analysis of Mg-Ce alloy after severe plastic deformation, 26th International Conference on Metallurgy and Materials, Conference Proceedings.

[32] C. W. Su, L. Lu, M. O. Lai. Recrystallization and grain growth of deformed magnesium alloy. Philos. Mag. 88 (2008) 181–200. https://doi.org/10.1080/14786430701805566

[33] P. G. Boswell. On the calculation of activation-energies using a modified Kissinger method, J. Therm. Anal. 18(1980) 353–358. https://doi.org/10.1007/BF02055820

[34] X. Sauvage, S. Mukhtarov. Microstructure evolution of a multiphase super alloy processed by severe plastic deformation. IOP Conf. Series: Materials Science and Engineering 63 (2014) 012173. https://doi.org/10.1088/1757-899X/63/1/012173

[35] S. A. Alsubaie, Y. Huang, T. G. Langdon. Hardness evolution of AZ80 magnesium alloy processed by HPT at different temperatures. J. Mater. Res. Technol. 6 (2017) 378–384. https://doi.org/10.1016/j.jmrt.2017.05.004

[36] H. Wang, K. Zhou, G. Xie, X. Liang, W. Liang, Y. Zhao. Microstructure and mechanical properties of an Mg–10Al alloy fabricated by Sb-alloying and ECAP processing. Mater. Sci. Eng. A 560 (2013) 787–791. https://doi.org/10.1016/j.msea.2012.10.036

[37] Y. Cao, S. Ni, X. Liao, M. Song, Y. Zhu. Structural evolutions of metallic materials processed by severe plastic deformation. Mater. Sci. Eng. R 133 (2018) 1–59. https://doi.org/10.1016/j.mser.2018.06.001

[38] L.L. Rokhlin. Magnesium alloys containing rare earth metals, Taylor & Francis, New York (2003). p. 99.

[39] H.J. Frost, M.F. Ashby. Deformation Mechanism Maps. Pergamon, Oxford, U.K, (1982).

[40] Q. Li , X. Jiao. Recrystallization mechanism and activation energies of severely-deformed magnesium during annealing process. Materialia 000 (2019) 100188. https://doi.org/10.1016/j.mtla.2018.100188

[41] D. Setman, E. Schafler, E. Korznikova, M.J. Zehetbauer. The presence and nature of vacancy type defects in nanometals detained by severe plastic deformation. Mater. Sci. Eng. A 493 (2008)116–122. https://doi.org/10.1016/j.msea.2007.06.093

[42] Q. Miao, L. Hu, X. Wang, E. Wang. Grain growth kinetics of a fine-grained AZ31 magnesium alloy produced by hot rolling. J. Alloy. Compd.493 (2010) 87–90. doi:10.1016/j.jallcom.2009.12.049

[43] T. Al-Samman, X. Li. Sheet texture modification in magnesium-based alloys by selective rare earth alloying. Mater. Sci. Eng. A 528 (2011) 3809–3822. https://doi.org/10.1016/j.msea.2011.01.080

[44] H. Azzeddine, D. Bradai. On the Texture and Grain Growth in Hot Deformed and Annealed WE54 Alloy. International Journal of Materials Research, 11 (2012) 1351–1360. https://doi.org/10.3139/146.110768

[45] R. Alizadeh, R. Mahmudi, A. H. W. Ngan, T. G. Langdon. Microstructural stability and grain growth kinetics in an extruded fine-grained Mg–Gd–Y–Zr alloy. J. Mater. Sci. 50 (2015) 4940–4951. https://doi.org/10.1007/s10853-015-9041-x

[46] L.R.C. Malheiros, R. B. Figueiredo, T. G. Langdon. Grain size and microhardness evolution during annealing of a magnesium alloy processed by high-pressure torsion. Journal

of Materials Research and Technology. 4 (2015) 14–17. https://doi.org/10.1016/j.jmrt.2014.10.008

[47] J. Su, M. Sanjari, A. S. H. Kabir, J. J. Jonas, S. Yue. Static recrystallization behavior of magnesium AZ31 alloy subjected to high speed rolling. Mater. Sci. Eng. A 662 (2016) 412–425. https://doi.org/10.1016/j.msea.2016.03.047

[48] I. Basu, T. Al-Samman, Triggering rare earth texture modification in magnesium alloys by addition of zinc and zirconium, Acta Mater. 67 (2014) 116–133. https://doi.org/10.1016/j.actamat.2013.12.015

[49] I. Basu, T. Al-Samman, G. Gottstein. Shear band-related recrystallization and grain growth in two rolled magnesium-rare earth alloys. Mater. Sci. Eng. A 579 (2013) 50–56. https://doi.org/10.1016/j.msea.2013.04.076

[50] N. Stanford, M.R. Barnett. The origin of "rare earth" texture development in extruded Mg-based alloys and its effect on tensile ductility. Mater. Sci. Eng. A 496 (2008) 399–408. https://doi.org/10.1016/j.msea.2008.05.045

[51] D. Ahmadkhaniha, Y. Huang, M. Jaskari, A. Järvenpää, M. H. Sohi, C. Zanella, L. P. Karjalainen, T. G. Langdon. Effect of high-pressure torsion on microstructure, mechanical properties and corrosion resistance of cast pure Mg. J. Mater. Sci. 53 (2018) 16585–16597. https://doi.org/10.1007/s10853-018-2779-1

[52] Y. I. Bourezg, H. Azzeddine, T. Baudin, A-L Helbert, Y. Huang, D. Bradai, T. G. Langdon. Texture and microhardness of Mg-Rare Earth (Nd and Ce) alloys processed by high-pressure torsion. Mater. Sci. Eng. A 724 (2018) 477–485. https://doi.org/10.1016/j.msea.2018.03.114

[53] S. Abdessameud, D. Bradai. Microstructure and Texture Evolution in Hot Rolled and Annealed Magnesium Alloy TRC AZ31. Can. Metall. Quart. 48 (2009) 433–442. https://doi.org/10.1179/cmq.2009.48.4.433

[54] S. Abdessameud, H. Azzeddine, B. Alili, D. Bradai. On the grain growth in AZ31 alloy after uniaxial compression. Trans. Nonferrous Met. Soc. China 20 (2010) 2215–2222. https://doi.org/10.1016/S1003-6326(10)60631-0

[55] T. Al-Samman, G. Gottstein. Dynamic recrystallization during high temperature deformation of magnesium. Mater. Sci. Eng. A 490 (2008) 411–420. https://doi.org/10.1016/j.msea.2008.02.004

[56] Y. Huang, R.B. Figueiredo, T. Baudin, A.-L. Helbert, F. Brisset, T.G. Langdon, Microstructure and texture evolution in a magnesium alloy during processing by high-pressure torsion, Mater. Res. 16 (2013) 577–585. http://dx.doi.org/10.1590/S1516-14392013005000025

[57] T. Al-Samman, B. Ahmad, G. Gottstein, Uniaxial and plane strain compression behavior of magnesium alloy AZ31: A comparative study, Mater. Sci. Forum 550 (2007) 229–234. https://doi.org/10.4028/www.scientific.net/MSF.550.229

[58] A. Imandoust, C.D. Barrett, T. Al-Samman, K.A. Inal, H. El Kadiri, A review on the effect of rare-earth elements on texture evolution during processing of magnesium alloys, J. Mater. Sci. 52 (2017) 1–29. https://doi.org/10.1007/s10853-016-0371-0

[59] C. D. Barrett, A. Imandoust, A. L. Oppedal, K. Inal, M. A. Tschopp, H. El Kadiri. Effect of grain boundaries on texture formation during dynamic recrystallization of magnesium alloys. Acta Mater. 128 (2017) 270–283. https://doi.org/10.1016/j.actamat.2017.01.063

[60] R.D. Doherty. Nucleation and growth kinetics of different recrystallization texture components. Scr. Metall. 19 (1985) 927–930. https://doi.org/10.1016/0036-9748(85)90284-4

[61] C.D. Barrett, A. Imandoust, H. El Kadiri. The effect of rare earth element segregation on grain boundary energy and mobility in magnesium and ensuing texture weakening. Scr. Mater. 146 (2018) 46–50. https://doi.org/10.1016/j.scriptamat.2017.11.004

[62] M.G. Jiang, C. Xu, H. Yan, S. H. Lu, T. Nakata, C. S. Lao, R. S. Chen, S. Kamado, E. H. Han. Correlation between dynamic recrystallization and formation of rare earth texture in a Mg-Zn-Gd magnesium alloy during extrusion. Scientific Reports (2018) 8:16800. DOI:10.1038/s41598-018-35170-4

[63] Z.R. Zeng, Y.M. Zhu, S.W. Xu, M.Z. Bian, C.H.J. Davies, N. Birbilis, J.F. Nie. Texture evolution during static recrystallization of cold-rolled magnesium alloys. Acta Mater. 105 (2016) 479–494. https://doi.org/10.1016/j.actamat.2015.12.045

[64] B.L. Wu, Y.H. Zhao, X.H. Du, Y.D. Zhang, F. Wagner, C. Esling. Ductility enhancement of extruded magnesium via yttrium addition. Mater. Sci. Eng. A 527 (2010) 4334–4340. https://doi.org/10.1016/j.msea.2010.03.054

[65] Y.B. Chun, C.H.J. Davies. Texture effect on microyielding of wrought magnesium alloy AZ31. Mater. Sci. Eng. A 528 (2011) 3489–3495. https://doi.org/10.1016/j.msea.2011.01.046

[66] F. Abouhilou. A.Hanna, H. Azzeddine, D. Bradai. Microstructure and texture evolution of AZ31 Mg alloy after uniaxial compression and annealing. Journal of Magnesium and Alloys, in press Available online 27 December 2018. https://doi.org/10.1016/j.jma.2018.11.003

[67] J. Koike, T. Kobayashi, T. Mukai, H. Watanabe, M. Suzuki, K. Maruyama, K. Higashi, The activity of non-basal slip systems and dynamic recovery at room temperature in fine-grained AZ31B magnesium alloys, Acta Mater. 51 (2003) 2055–2065. https://doi.org/10.1016/S1359-6454(03)00005-3

Highlights

- Processing by HPT up 5 turns produces a significant refinement in grain size.
- The recrystallization temperature was measured in the range of ~120–200 °C.
- The activation energy for recrystallization was ~25 kJ mol^{-1}.
- The texture was retained after subsequent annealing at 400 °C for 1 h.
- A good thermal stability was demonstrated after annealing at 400 °C for 1 h.